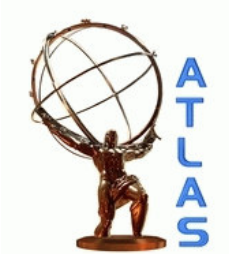

ATLAS CSC NOTE

ATL-PHYS-PUB-2009-000

April 24, 2009

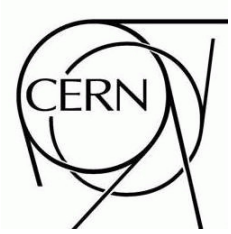

Muons in the Calorimeters: Energy Loss Corrections and Muon Tagging

The ATLAS Collaboration[1)]

This note is part of CERN-OPEN-2008-020. This version of the note should not be cited: all citations should be to CERN-OPEN-2008-020.

Abstract

The muon spectrometer is the outermost subdetector of the ATLAS detector, beginning after a muon has traversed 100 radiation lengths of material. Muon momentum measurements must be corrected for energy loss in the calorimeters and the inert material before the muons reach the muon spectrometer. Energy lost in the calorimeters can be estimated from parameterizations or from a measurement of the energy deposited in the calorimeters. In addition, the muon energy loss measurement can be used to tag muons not reconstructed in the muon spectrometer due to inefficiencies, spectrometer acceptance or their low momenta.

In this document we discuss different algorithms developed to perform the energy loss correction in the muon reconstruction. We compare the performance of the muon reconstruction algorithms before and after the energy loss correction is applied. In addition, we describe the muon tagging algorithms, based on measurements obtained in the calorimeters, and contrast their performance in different simulated data samples.

[1)] This note prepared by K.A. Assamagan, K. Bachas, T. Carli, T. Davidek, D. Fassouliotis, L. R. Flores Castillo, N. de Groot, S. Hassani, E.W. Hughes, P. Kluit, I. Korolkov, C. Kourkoumelis, J.-F. Laporte, H. Lim, M. Limper, D. López Mateos, B. Mellado Garcia, K. Nikolopoulos, C. Petridou, A. Poppleton, L. Pribyl, G. Ordóñez Sanz, A. Ouraou, M. Ridel, D. Rousseau, A. Ruiz-Martinez, O. Salto, A. Salzburger, G. Schlager, P. Schwemling, G. Usai and S.L. Wu.

1 Introduction

Muons traverse the inner detector and the calorimeters in the ATLAS experiment before reaching the muon spectrometer. The material thickness traversed by the muons before reaching the muon spectrometer is over 100 radiation lengths (X_0) (see Figure 1). By passing through this material, muons undergo electromagnetic interactions which result in a partial loss of their energy. As over 80% of this material is in the instrumented areas of the calorimeters, the energy loss can be measured. Understanding how this energy loss happens, its magnitude and how to measure it is essential to obtain the best performance in muon reconstruction and identification.

In this document we discuss the aspects of muon reconstruction and identification that make use of all available energy loss information in the ATLAS software. The Muonboy [1] and Muid [2] algorithms for muon reconstruction take into account internally the calorimeter material effects for tracks already found in the muon spectrometer. Algorithms that calculate the energy loss and transport the track anywhere in the detector are also available. The detailed computation of this correction is the main focus of Sections 2 and 3, while Section 4 is devoted to the use of the energy loss information for muon identification. This note gives an overview of the current algorithms and techniques which will be used for the reconstruction of the first data.

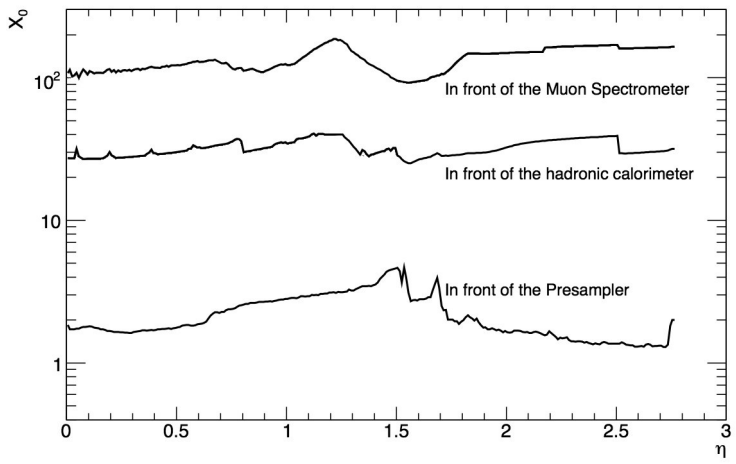

Figure 1: Material distribution before the muon spectrometer in ATLAS as a function of η [3]. The material is expressed in radiation lengths (X_0).

2 Algorithmic Treatment of Material Effects

When a muon traverses the detector material, it undergoes successive deflections and a loss of energy. The total angular deflection is an accumulation of many small angle deflections, referred to as multiple (Coulomb) scattering; and it is well approximated by a gaussian distribution that is centered at a zero mean value. The expected root mean square of the projected scattering angle can be described by the formula of Highland [4]:

$$\sigma_{ms}^{proj} = \frac{13.6\ \text{MeV}}{\beta cp}\sqrt{t}[1+0.038\ln t], \tag{1}$$

where t is the thickness of the traversed material in units of the radiation length X_0. The energy loss, on the other hand, is non-gaussian. Throughout this document, we will study the energy loss of muons going through the ATLAS detector in detail. The discussion of multiple scattering, however, will be limited

to this section, because it is simpler and it will be based on the Highland formula shown above. The thickness in the formula above is calculated from the geometry description for all algorithms. However, there are small differences in how the multiple scattering information is used in the track fitting. These differences are explained below, as the different track fitting strategies are discussed.

In ATLAS track reconstruction applications, two main track fitting strategies are deployed: the classical least squares method and the progressive method that corresponds to the Kalman filter formalism [5].

The least squares fit: In the global fitting technique, most material effects are directly integrated into the χ^2 function (the energy loss may or may not be fitted). This is done by introducing the deflection angles and, possibly, energy losses as additional parameters to the fit.

The contribution of the fitted scattering angles to the χ^2 function has to be regulated by the expected range of the scattering process in the traversed material. Scattering effects are applied to the muon on two surfaces along its trajectory, because the scattering effects from material bulk can be accurately described by two scattering centers. The Muonboy algorithm iterates its calculation of the muon trajectory in a complex geometry with many scattering centers. The number of scattering centers is reduced to two after the iteration. The iteration allows for a calculation of the material traversed after the trajectory has been modified to account for the energy loss. On the other hand, the Muid algorithm and the ATLAS tracking global-χ^2 fitter [6] currently use a map of the material from the Monte Carlo on two surfaces. The η coordinate of the track on these two surfaces is then used to calculate the amount of material traversed by the muon.

The least squares fit with the calorimeter energy loss as a fitted variable can only be performed in a combined fit including measurements of both the muon spectrometer segments and the inner detector hits. If no inner detector hits exist, the treatment of the energy loss effects is fundamentally equivalent for both a least-squares-inspired algorithm and a Kalman-filter-inspired algorithm.

To minimize the number of degrees of freedom in the least-squares fit, the number of fitted variables must be minimized. In particular, one energy loss variable in a track fit is preferable. This does not mean that the trajectory cannot be affected smoothly by the energy loss, because an extended set of material layers can be calculated using a detailed detector description as in Figure 2 and the fitted energy loss distributed proportionally among these layers. This is done for the purpose of transporting the track through the calorimeters inside the Muonboy algorithm. An alternative approach is currently taken in the Muid and ATLAS tracking global-χ^2 fitter. These algorithms apply the energy loss to the track on one surface inside the calorimeters hence approximate the rate of change of curvature within the calorimeter volume (i.e.: they assume the momentum of the muon changes only at one place along its trajectory).

The effect of this simplification on the muon combined reconstruction is expected to be small, because the energy loss only affects the trajectory of the track if the track is bending. However, the area where most of the energy loss happens (the calorimeter) has a small magnetic field. A quantitative estimate of the effect of the simplification can be obtained by comparing the multiple scattering effects on the track and the bending that the track undergoes from its entrance in the calorimeters to its exit. The bending is shown in Figure 3. Equation 1 indicates that a 10 GeV (100 GeV) muon going through the calorimeters scatters following a gaussian distribution with RMS $\approx$14-20 (1.4-2) milliradians (with $X_0 =$ 100-200 from Figure 1). Figure 3 shows that the deviation of the track due to the magnetic field is comparable to the deviation expected from multiple scattering at least in the ϕ direction. Algorithms that use one surface to apply the energy loss correction approximate the mean trajectory inside the calorimeter with a systematic offset that increases with depth to a maximum value at the calorimeter centre. The magnitude of this offset is proportional to the magnetic bending scaled by the fraction of energy loss to muon energy. It thus remains small with respect to the uncertainties caused by Coulomb scattering.

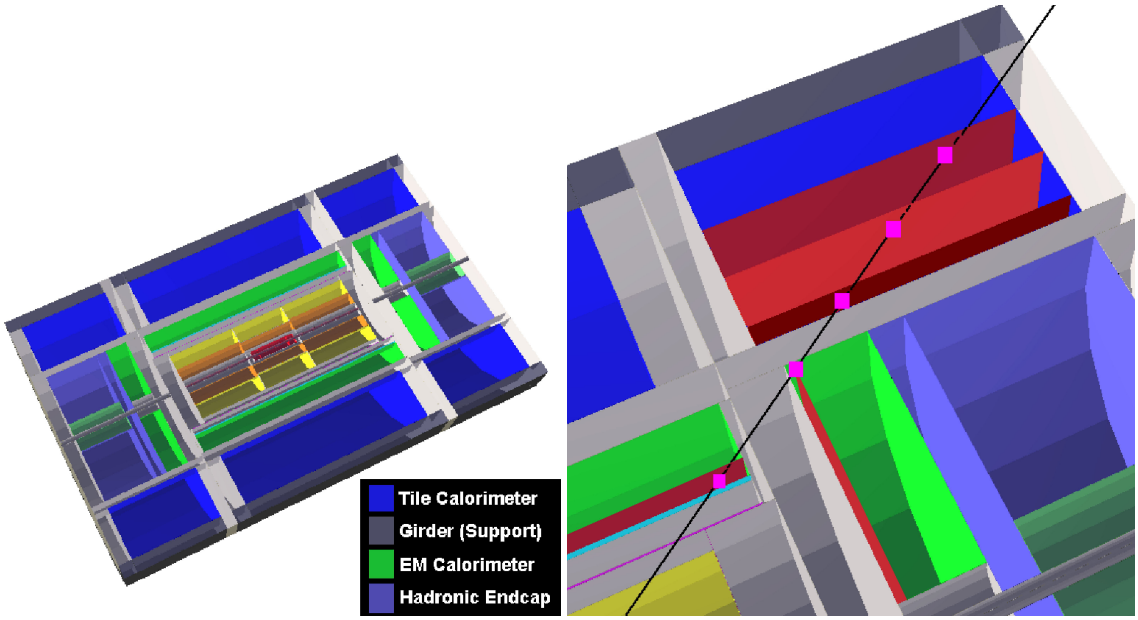

Figure 2: Left: 3-D view of the tracking geometry up to the muon spectrometer. Right: Example set of energy loss update layers (shown as additional surfaces with respect to the figure on the left; update positions shown as squares) created during the extrapolation of a track (black line) through the calorimeter.

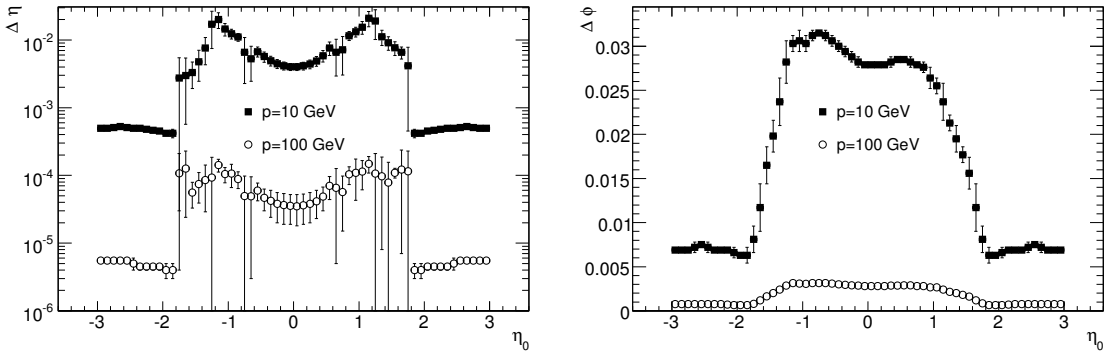

Figure 3: Calculated difference between the calorimeter entrance and exit coordinates ($\Delta\eta$, left, and $\Delta\phi$, right) for 10 GeV (solid squares) and 100 GeV muons as a function of η_0 of the muon at the interaction point. The lack of mirror symmetry is due to the combined effect of the return flux of the solenoid (unidirectional) and the toroidal magnetic field (symmetric around the z axis).

Progressive fitting techniques: In progressive fitting techniques, the particle-detector interaction is part of the transport process of the track to the next surface where a hit may exist (measurement surface). The transported track can then be compared (and updated) with the measurement obtained on the next measurement surface. In this transport process magnetic field and material effects (multiple scattering and energy loss) are applied to the parameterization of the track. Multiple scattering is applied by increasing the uncertainties of the angular direction variables, while energy loss effects are taken into account in two ways. A mean energy loss is applied to the track parameterization, and then an uncertainty is added to the corresponding covariance matrix term to account for the stochastic behavior of the

energy loss. The resulting increased covariance terms degrade the track prediction for the subsequent measurement surface.

Progressive fitting tools rely, therefore, on a precise description of the detector material and magnetic field. An example is shown in Figure 2. The illustration on the right of Figure 2 shows material layers that are calculated dynamically during the extrapolation process into the calorimeter active volumes.

In ATLAS, the stand-alone muon reconstruction algorithms (MOORE [7] and Muonboy) use exclusively the least-squares formalism to fit tracks in the muon spectrometer. On the other hand, the inner detector reconstruction uses by default the progressive fitting techniques. In combined muon reconstruction, when the hits in the inner detector are used in combination with the muon spectrometer, the Muonboy-based algorithm (STACO) combines tracks reconstructed in the inner detector and muon spectrometer independently, therefore being a mixture of the tracking fit and the least-squares fit carried out by Muonboy. On the other hand, the MOORE-based algorithm (Muid) performs a least-squares fit in both subsystems.

3 Corrections for the Energy Loss from the Beam Pipe to the Muon Spectrometer

In this section we describe how the energy loss is calculated from GEANT4 [8] based parameterizations and/or measurements of the energy loss by the calorimeters. Muon isolation is also discussed in this context. Finally, the energy loss corrections are validated as part of the muon reconstruction algorithms.

3.1 Parameterizations of the Energy Loss

Relativistic muons going through matter lose energy mostly through electromagnetic processes: ionization, e^+e^- pair-production, and bremsstrahlung. Ionization energy loss dominates for muons of momenta $\lesssim$100 GeV. Bremsstrahlung and e^+e^- pair-production energy losses are often jointly referred to as radiative energy losses. Higher energy muons lose energy mostly through radiative energy losses. However, when passing through materials made of high-Z elements the radiative effects can be already significant for muons of energies $\approx$10 GeV [9].

Ionization energy losses have been studied in detail, and an expression for the mean energy loss per unit length as a function of muon momentum and material type exists in the form of the Bethe-Bloch equation [10]. Other closed-form formulae exist to describe other properties of the ionization energy loss. Bremsstrahlung energy losses can be well parameterized using the Bethe-Heitler equation. However, there is no closed-form formula that accounts for all energy losses. Nevertheless, theoretical calculations for the cross-sections of all these energy loss processes do exist. With these closed-form cross-sections, simulation software such as GEANT4 can be used to calculate the energy loss distribution for muons going through a specific material or set of materials.

The fluctuations of the ionization energy loss of muons in thin layers of material are characterized by a Landau distribution. Here "thin" refers to any amount of material where the muon loses a small percentage of its energy. Once radiative effects become the main contribution to the energy loss, the shape of the distribution changes slowly into a distribution with a larger tail. Fits to a Landau distribution still characterize the distribution fairly well, with a small bias that pushes the most probable value of the fitted distribution to values higher than the most probable energy loss [11]. These features are shown for the energy loss distributions of muons going from the beam-pipe to the exit of the calorimeters in Figure 4.

As can be seen in Figure 4 the Landau distribution is highly asymmetrical with a long tail towards higher energy loss. For track fitting, where most of the common fitters require gaussian process noise,

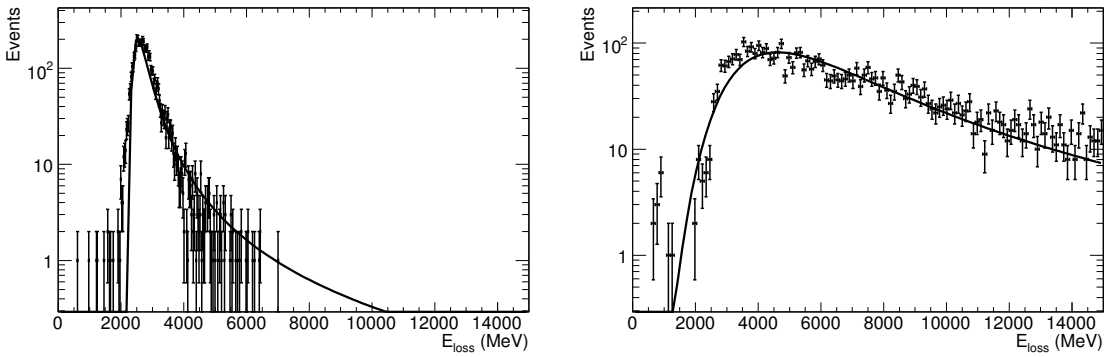

Figure 4: Distribution of the energy loss of muons passing through the calorimeters ($|\eta| < 0.15$) as obtained for 10 GeV muons (left) and 1 TeV muons (right) fitted to Landau distributions (solid line).

this has a non-trivial consequence: in general, a gaussian approximation has to be performed for the inclusion of material effects in the track fitting [12].

In order to express muon spectrometer tracks at the perigee, the total energy loss in the path can be parameterized and applied to the track at some specific position inside the calorimeters. As the detector is approximately symmetric in ϕ, parameterizations need only be done as a function of muon momentum and η. The η-dependence is included by performing the momentum parameterizations in different η bins of width 0.1 throughout the muon spectrometer acceptance ($|\eta| < 2.7$). The dependence of the most probable value of the energy loss, $E_{\rm loss}^{\rm mpv}$, as a function of the muon momentum, p_μ, is well described by

$$E_{\rm loss}^{\rm mpv}(p_\mu) = a_0^{\rm mpv} + a_1^{\rm mpv} \ln p_\mu + a_2^{\rm mpv} p_\mu, \tag{2}$$

where $a_0^{\rm mpv}$ describes the minimum ionizing part, $a_1^{\rm mpv}$ describes the relativistic rise, and $a_2^{\rm mpv}$ describes the radiative effects. The width parameter, $\sigma_{\rm loss}$, of the energy loss distribution is well fitted by a linear function $\sigma_{\rm loss}(p_\mu) = a_0^\sigma + a_1^\sigma p_\mu$. Some of these fits are illustrated in Figure 5. This parameterization is

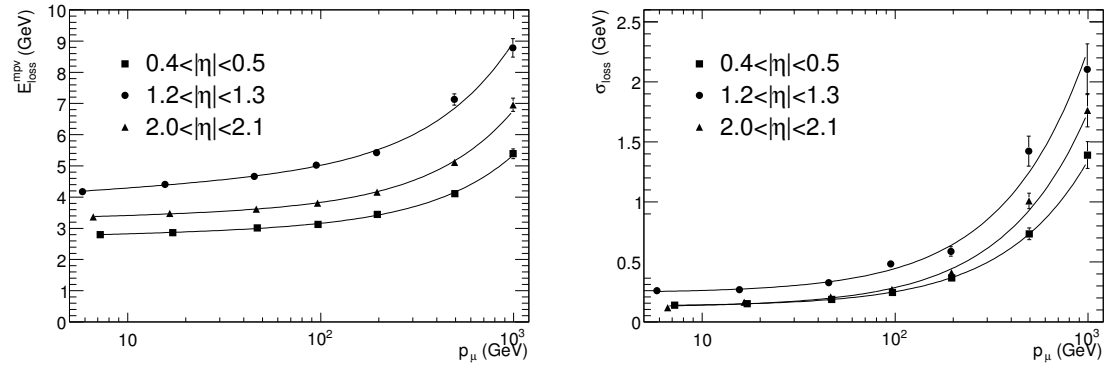

Figure 5: Parameterization of the $E_{\rm loss}^{\rm mpv}$ (left) and $\sigma_{\rm loss}$ (right) of the Landau distribution as a function of muon momentum for different η regions. One sees a good agreement between the GEANT4 values and the parameterization.

used as part of the Muid algorithm for combined muon reconstruction [3].

An alternative approach exists in the ATLAS tracking. In this approach, the energy loss is parameterized in each calorimeter or even calorimeter layer. The parameterization inside the calorimeters is applied to the muon track using the detailed geometry described in Section 2.

The most probable value and width parameter of the Landau distribution are not affected by radiative energy losses in thin materials in the muon energy range of interest ($\sim$5 GeV to a few TeV). This justifies treating energy loss in non-instrumented material, such as support structures, up to the entrance of the muon spectrometer as if it was caused by ionization processes only. The most probable value of the distribution of energy loss by ionization can be calculated if the distribution of material is known [13]. Since material properties are known in each of the volumes in the geometry description used, it is easy to apply this correction to tracks being transported through this geometry.

For the instrumented regions of the calorimeters, a parameterization that accounts for the large radiative energy losses is required. To provide a parameterization that is correct for the full η range and for track transport inside the calorimeters, a study of energy loss as a function of the traversed calorimeter thickness, x, was performed. Two parameters that characterize fully the pdf of the energy loss for muons were fitted satisfactorily using several fixed momentum samples as

$$E_{\rm loss}^{\rm mpv,\sigma}(x,p_\mu) = b_0^{\rm mpv,\sigma}(p_\mu)x + b_1^{\rm mpv,\sigma}(p_\mu)x\ln x. \tag{3}$$

The momentum dependence of the $b_i(p_\mu)$ parameters was found to follow the same form as in Equation 2. Fits for some of the absorber materials are shown in Figure 6. These parameterizations have

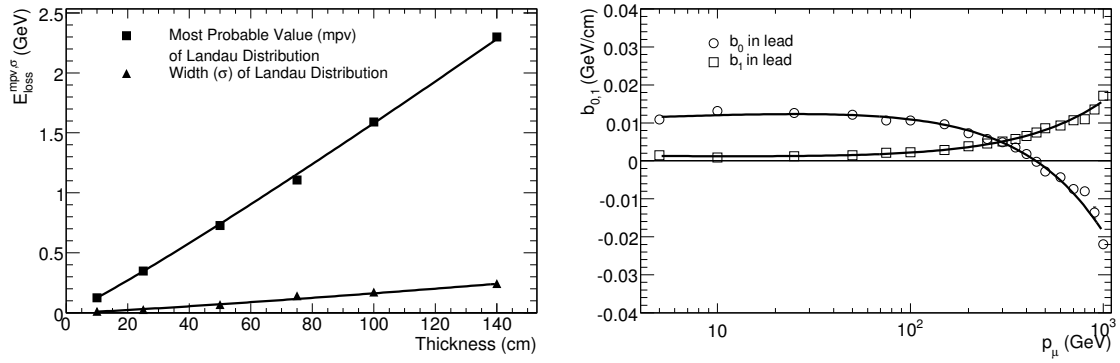

Figure 6: Left: Fit to the most probable value and width of the Landau distribution as a function of thickness of iron for muons of momentum 200 GeV. The fitting function has the form $b_0x + b_1x\ln x$. Right: Fit to the parameters b_0 and b_1 for the most probable value of the energy loss in lead as a function of muon momentum.

been validated over the η range from -3 to 3. A direct comparison of the most probable energy loss in GEANT4 simulation and in the geometry of the ATLAS tracking algorithms is shown in Figure 7 for muons propagating from the beam-pipe to the exit of the electromagnetic calorimeters and to the exit of the hadronic calorimeters.

3.2 Measurements of the Energy Deposited in the Calorimeters

In this section the measurement of the muon energy loss in the calorimeters is discussed. Understanding this measurement is important because it allows for an improvement in the energy loss determination. This section provides a basic description of the ATLAS calorimeters and their measurements which is important for understanding the topics discussed in Sections 3.3, 3.4 and 4.

3.2.1 Muons in the Liquid Argon Calorimeters

The electromagnetic calorimeter is a lead-liquid argon sampling calorimeter with accordion shaped absorbers and electrodes, covering the $|\eta|$ range up to 3.2.

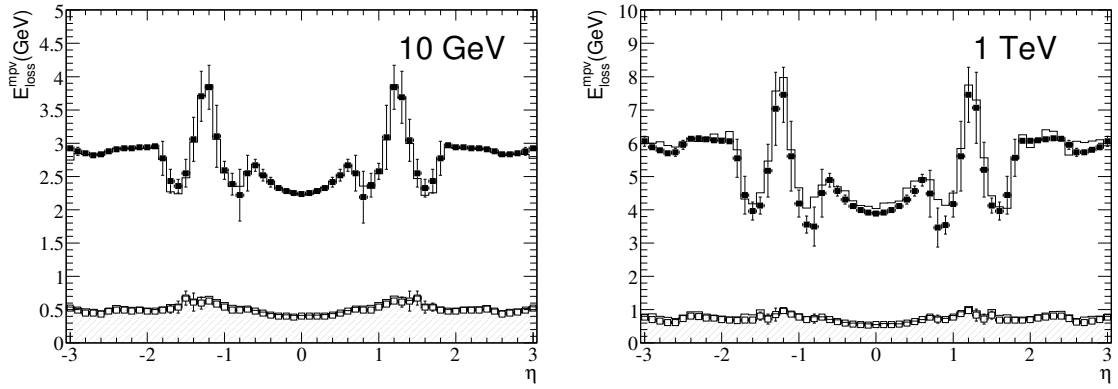

Figure 7: Most probable value of the energy loss as parameterized in the geometry of the ATLAS tracking (points) and in GEANT4 for muons of momentum 10 GeV (left) and 1 TeV (right) as a function of pseudorapidity. The solid line and points correspond to the energy loss of muons propagating from the beam pipe to the exit of the hadronic calorimeters. The filled histogram and hollow points correspond to the energy loss of muons propagating from the beam pipe to the entrance of the hadronic calorimeters.

The hadronic end-cap calorimeter, also based on liquid argon technology, covers the $|\eta|$ range from 1.5 to 3.2. The absorbers are made of parallel plates of copper. The total thickness of the hadronic end-cap calorimeters is 10 interaction lengths (λ_{int}). The measurement of a muon signal in the hadronic end-cap is complicated because the noise levels are high compared to the muon signal itself [14].

The detailed geometrical description of the LAr calorimeters is presented in [15]. Only the aspects relevant for muon studies will be recalled. Both barrel and end-cap calorimeters possess up to three longitudinal samplings (called strip, middle and back). They are completed by a liquid argon presampler detector to estimate the energy lost in upstream material. The signal and noise distributions in two longitudinal calorimeter samples in the barrel of the electromagnetic calorimeter are shown in Figure 8 for 150 GeV muons. Further discussion of how these distributions were calculated from the combined test beam data can be found in Section 4. The signal can be separated from the noise, especially in the middle sampling. In addition, comparisons between GEANT4 simulation and test beam data show that, despite the high noise in the first sampling, the electromagnetic calorimeter can measure reliably the energy lost by muons traversing it.

3.2.2 Muons in the Tile Calorimeter

The Tile Calorimeter (TileCal) [17] is a plastic scintillator/steel sampling calorimeter, located in the region $|\eta| < 1.7$; it is divided into three cylindrical sections, referred to as the barrel and extended barrels. It extends from an inner radius of 2.28 m to an outer radius of 4.25 m. Modules are segmented in η and in radial depth. In the direction perpendicular to the beam axis, the three radial segments span 1.5, 4.1 and 1.8 λ_{int} in the barrel and 1.5, 2.6, 3.3 λ_{int} in the extended barrels. The resulting typical cell dimensions are $\Delta\eta \times \Delta\phi = 0.1 \times 0.1$ (0.2×0.1 in the outermost layer). This segmentation defines a quasi-projective tower structure.

The TileCal response to high-energy muons follows a Landau-type distribution with characteristically long tails at high energies caused by radiative processes and energetic δ–rays. This response has been extensively studied in test beams with 180 GeV muons incident at projective angles. The peak values of the muon signals vary by more than a factor of two in projective geometry. An example of the muon signal, expressed in units of collected charge (pC), is shown in Figure 9, both for the whole tower and the last radial compartment. The signal is well separated from the noise, with a signal-to-noise ratio

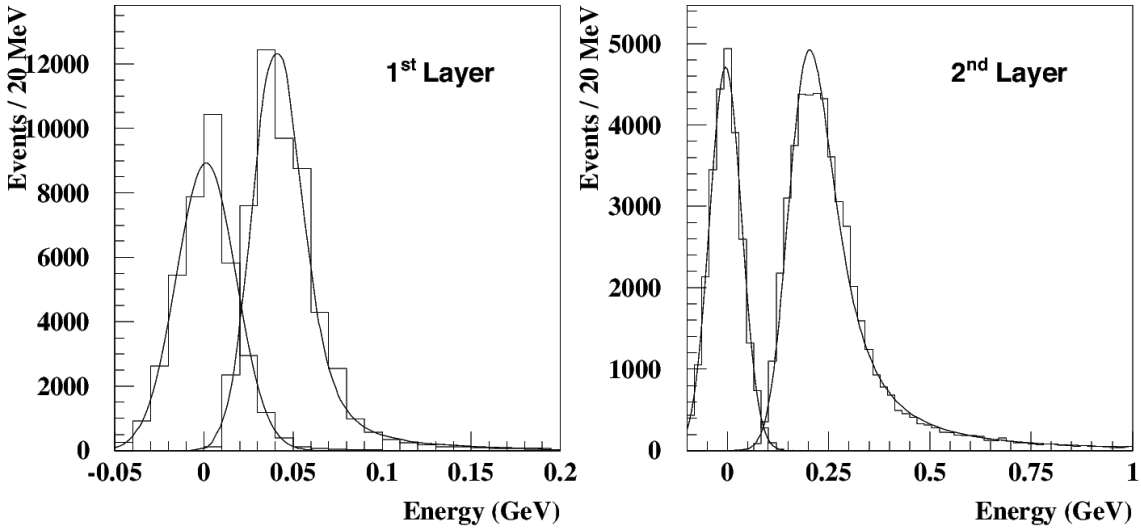

Figure 8: Distribution of the muon energy deposited in one electromagnetic calorimeter cell by 150 GeV muons, fitted to a Landau function convolved with a gaussian [16]. The gaussians on the left of each plot are the distributions of the noise. Left (right): energy deposit in a cell belonging to the first (middle) longitudinal sampling traversed by the muon. The energy is the sum of the energies of the (up to two) cells belonging to the muon cluster (see Section 4). The data were collected in the 2004 Combined Test Beam.

(S/N) of ~ 44 and ~ 18 respectively. The muon response was shown to be uniform in η to within 1.9 % over all modules tested. The energy deposition spectrum observed in the TileCal test beams is within a few percent of the GEANT4 prediction.

3.2.3 Measurements in Muon Algorithms

The previous sections discussed the reconstruction of energy depositions at the cell level. To provide estimates of muon energy loss and muon isolation, several cells need to be used along the muon trajectory. In addition, muon calibration factors such as the e/μ ratio for minimum ionizing muons, need to be adjusted in order to find the correct energy deposition.

The classical method for measuring the energy loss of muons in calorimeters is based on the concept of a calorimeter tower, where the muon is assumed to follow a straight trajectory inside the calorimeters. A tower is defined as all calorimeter cells within a cone of fixed radius $\Delta R = \sqrt{\Delta\eta^2 + \Delta\phi^2}$ centered around the muon trajectory. Motivated by this concept, but with a few muon-specific changes, the *Straight Line* method has been developed as part of the Muid algorithm for muon reconstruction. The Straight Line method calculates the coordinates of the relevant track at half the depth of the calorimeter by transporting the track to that position. These coordinates are used to calculate the calorimeter cells included in the measurement cone.

In the *Track Update* method, the muon trajectory through the calorimeters is extrapolated either from inner detector tracks or muon spectrometer tracks. Given this trajectory, the center of the measurement cone is recalculated at each calorimeter layer. Figure 10 shows a qualitative comparison between the Straight Line method and the Track Update method.

Figure 3 illustrated the quantitative differences in the muon trajectories from the two methods. The difference between the Straight Line and Track Update methods can be estimated by comparing the coordinates of the muon at the entrance of the electromagnetic calorimeters and at the exit of the hadronic calorimeters. The difference is clearly negligible for muons of $p_T > 100$ GeV, even though it can be as

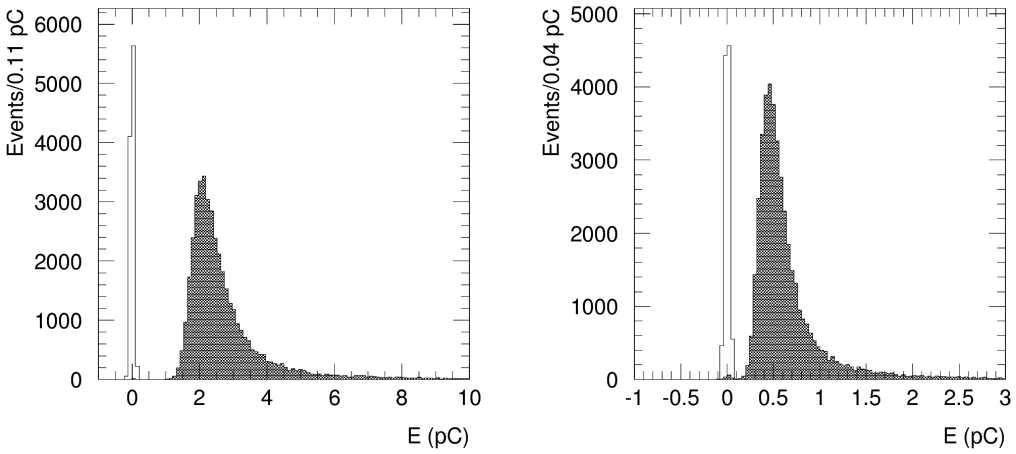

Figure 9: Example of the isolated muon signal as measured at $\eta = 0.35$ in the whole tower (left) and in the last radial compartment (right). The narrow peaks represent the corresponding noise. The energy is measured in units of collected charge. For a muon 1 pC corresponds to roughly 1 GeV, yielding a noise width of roughly 40 MeV for the last radial compartment. The data were collected in test beams in 2002 and 2003.

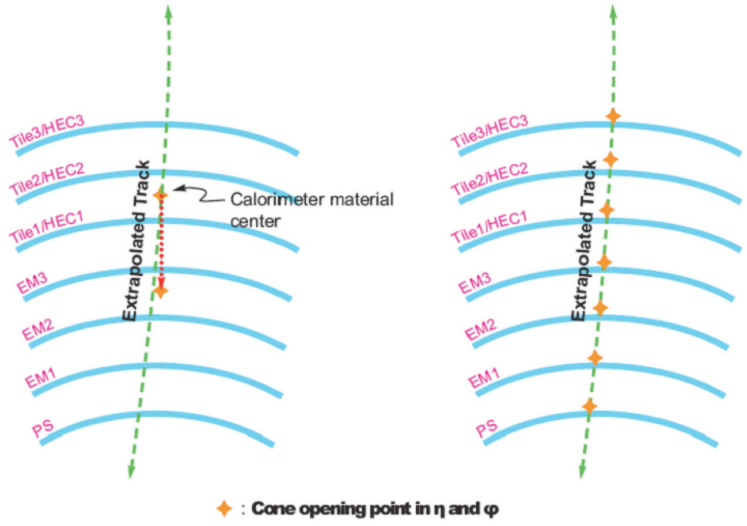

Figure 10: Illustration of the Straight Line (left) and Track Update (right) concepts.

big as a third of a hadronic cell width for 10 GeV muons.

In Figure 11, a comparison between the measured energy and the true energy loss is shown for the Track Update method. The average measured transverse energy loss in a cone of 0.2 around the muon trajectory for single muons of momentum 10, 100 and 300 GeV is shown as a function of η. In the same η bins the average true (as obtained from the GEANT4 full simulation) transverse energy lost between the interaction point and the entrance of the muon spectrometer is shown. The energy lost by the muons is well estimated by measurements in the calorimeters. The region around $|\eta| = 1$ corresponds to the crack in the TileCal. Consequently, the measurement underestimates the energy loss in that region.

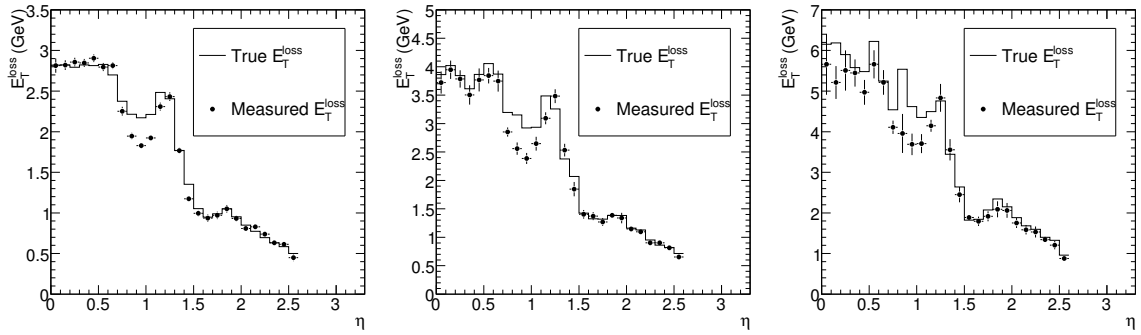

Figure 11: Comparison between the average measured transverse energy deposition (points) and true energy lost between the beam-pipe and the muon spectrometer (line) for muons of momentum 10 GeV (left), 100 GeV (center) and 300 GeV (right). The errors shown are statistical only.

3.3 Muon Isolation

The previous studies demonstrate the capabilities of the calorimeters to measure the energy lost by muons. However, these studies were all performed with single muon samples. In real physics samples, muons do not reach the calorimeters alone, but are often accompanied by additional particles that deposit energy in the cells around the muon trajectory and contaminate the muon energy loss measurement. Therefore, in order to determine the energy loss of such muons, isolation criteria must also be defined and optimized for maximum reliability in the energy measurement.

Isolation criteria can be divided into two categories: calorimeter-based and track-based. In muon reconstruction an area is defined around the muon trajectory with a minimum and maximum radius for the purpose of determining calorimeter isolation. This achieves the purpose of excluding the cells where the muon deposits its energy. The size of this inner radius needs to be optimized to collect most of the energy lost by the muon but as little energy as possible from other particles. The energy deposited in the annulus between the inner radius and the outer radius, where the muon deposits little energy, is what the following paragraphs refer to as *isolation energy*. The optimal radii that define this annulus depend on the underlying event and luminosity. However, the muon shower is contained in a small cone of radius ≈ 0.1 [18]. Therefore, a choice of an inner radius much bigger than 0.1 does not achieve the purpose of collecting the energy deposited by the muon, and it adds noise to the measurement.

A study to determine possible isolation criteria [3] has been performed on a fully simulated $t\bar{t}$ sample, where the W bosons were forced to decay into a muon and a neutrino. Muons produced by the semi-leptonic decays of b quarks tend to be non-isolated, while those from W decays tend to be isolated. In Figure 12 the distribution of the isolation energy for muons originating from quarks and Ws is shown for the electromagnetic and hadronic calorimeters. The isolation energy inner and outer radii are 0.075 (0.15) and 0.15 (0.30) for the electromagnetic (hadronic) calorimeters, respectively. This reflects their different granularities. The electromagnetic isolation energy is a more powerful discriminant for the annuli radii chosen.

Based on this figure, for the purpose of the rest of the studies in this section, a cut of 2 GeV on electromagnetic isolation was used to discriminate isolated muons from non-isolated muons. An additional cut of 10 GeV in hadronic isolation was used, even though this cut does not help rejecting non-isolated muons in the vast majority of events. These cuts were relaxed slightly with increasing muon p_T to account for a possible slight increase of the transverse radius of the shower caused by muons in the calorimeters.

Tracking-based criteria can be used to determine isolation cuts independent of calorimeter-based

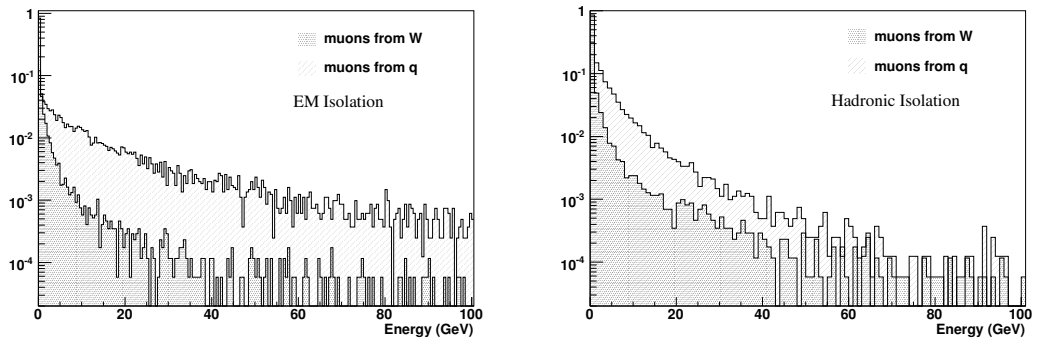

Figure 12: Distribution of the isolation energy in the electromagnetic ($0.075 < \Delta R < 0.15$) (left) and hadronic calorimeters ($0.15 < \Delta R < 0.30$) (right) in muons from a $t\bar{t}$ sample without pile-up.

criteria. If used together, they can help eliminate non-isolated muons belonging to highly-collimated jets that escape being identified by calorimeter-based criteria. In Figure 13 the number of inner detector tracks around the muon are plotted for muons from quarks and Ws in the same samples used for Figure 12. These distributions were obtained for muons that passed the calorimeter-based isolation cuts mentioned above.

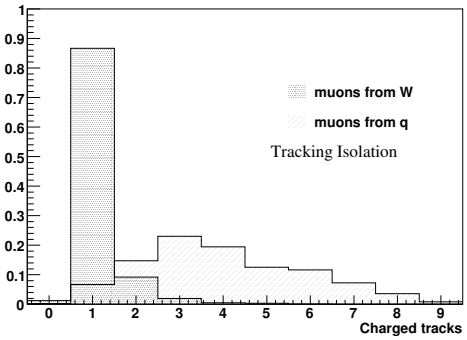

Figure 13: Distribution of the number of inner detector tracks (including the muon track) with $\Delta R < 0.2$ around the muon spectrometer track, after the calorimeter isolation and p_T threshold cuts are applied to muons in a $t\bar{t}$ sample.

The production rate of low-p_T non-isolated muons from b-quark decays is expected to be very significant. At the same time, a typical muon from a W or Z decay, will have a p_T of about 40 GeV. Thus, it is unlikely that low momentum muons will be isolated in a $t\bar{t}$ sample. For this reason, all muons with a p_T of less than 15 GeV were automatically tagged as non-isolated and are excluded. In most cases, the muon originating from a W boson is not accompanied by other tracks in the inner detector. In fact, the only track found in the track isolation cone is, essentially, the muon itself as reconstructed in the inner detector. In contrast, several inner detector tracks can be found close to muons originating from quarks. For an isolation cone of ΔR=0.2, the most probable value is three tracks, including the muon itself, but it can be much larger. A cut on tracking isolation has been applied that complements the cut on calorimeter isolation. This cut constrains an isolated muon track to be accompanied by at most one extra track inside the tracking isolation cone. Using the criteria described above (electromagnetic and hadronic calorimeter isolation, track isolation and $p_T^{\mu} > 15$ GeV) approximately 0.2% of the muons originating from b quarks have an energy loss overestimated by more than 6 GeV. On the other hand, 80% of the muons originating

from Ws are tagged as isolated.

All the cuts mentioned above are used by default as isolation criteria in the Muid muon reconstruction algorithm, to establish the contamination of the calorimeter measurement. If the cuts were not chosen tightly enough, non-isolated muons would exhibit an artificial increase in energy loss. If this measurement was then used in muon reconstruction, the reconstructed momentum at the interaction vertex would be artificially increased. This could significantly deteriorate the momentum measurement. A calorimeter measurement of the energy loss will then only make sense if the muon is tagged as isolated. These cuts were considered conservative enough that they could be used by default without inducing biases in the momentum reconstruction [3]. These cuts have not been studied with pile-up or in other samples with an important source of non-isolated muons, like high-p_T, $b\bar{b}$ samples. Studies of this type are important in order to set conservative isolation cuts as default for muon reconstruction involving calorimeter measurements.

In addition, it is worth discussing the relationship between muon isolation in reconstruction and muon isolation in physics analyses. While both concepts represent an attempt to determine whether a muon is inside a jet, analysis cuts are also decided on the basis of criteria such as efficiency or fake rate that are not necessarily important for the momentum reconstruction. It is, however, important to emphasize that the optimization of the cuts on reconstruction isolation for specific analyses is possible. It requires, nevertheless, a refitting of the track with analysis-specific cuts; and it should, therefore, only be attempted when the recovery of the Landau energy loss tails is crucial for the analysis and the standard treatment is not adequate.

For muon tagging, however, isolation criteria can overlap with the criteria derived for specific analyses. Isolation studies are necessary to provide a reliable muon tag and do not affect the momentum reconstruction, because the tracking algorithms are independent of the tagger. Default isolation criteria can, for example, be relaxed based on information from the physics sample and the specific analysis. As an example, Figure 14 shows the rejection on the $Zb\bar{b}$ background versus the Standard Model $H(130\text{ GeV}) \to ZZ^* \to \mu^+\mu^-\mu^+\mu^-$ efficiency using the calorimeter isolation cuts [19]. At this stage,

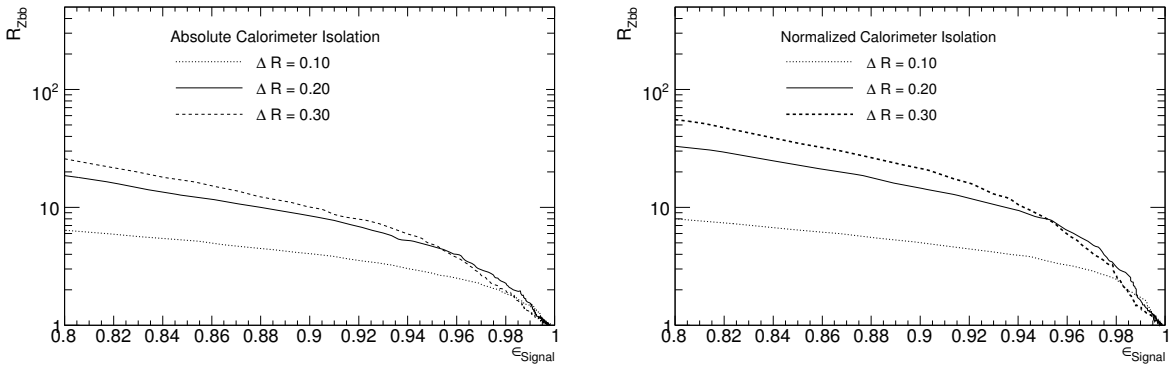

Figure 14: Rejection of the $Zb\bar{b}$ background as a function of the $H(130\text{ GeV}) \to 4\mu$ signal efficiency. Different radii ($0.1 < \Delta R < 0.3$) are compared for absolute, left, and normalized (with respect to muon p_T), right, calorimeter isolation. No pile up events were simulated.

after a preselection procedure, the four muon candidates have already been selected. Both absolute and normalized (with respect to muon p_T) isolation are presented. In these analyses, the isolation energy was defined using a cone of fixed radius. The isolation energy of an event was then defined as the isolation energy of the least isolated muon of the event. The optimum cone radius depends on signal efficiency, with ΔR of 0.2 being an efficient choice.

3.4 Measurement/Parameterization Combination Methods

To integrate energy loss in tracking algorithms, the energy loss is assumed to be gaussian. If the parameterization is used exclusively to correct for the energy loss, any event in which muons undergo a large energy loss will be incorrectly reconstructed. There is, thus, an advantage in using the parameterizations together with measurements in the calorimeters to optimize the energy loss reconstruction. Here we describe two algorithms developed to use the calorimeter information as well as the energy loss parameterizations for the muon reconstruction algorithms: the *Hybrid Method* [3] and the *Bayesian Method*. The Hybrid Method is used by default after isolation cuts as part of Muid. The Bayesian Method is used if specified by the user as part of Muonboy. By default, Muonboy uses a parameterization of the energy loss only.

The Hybrid Method consists in fully separating the two regions of the Landau distribution: the peak region and the tail region. The calorimetric energy loss measurement is used when the energy deposition is significantly larger than the most probable value (tail region); otherwise the parameterization is used (peak region). The transition point between the two regions is taken as $E_{\mathrm{mpv}} + 2\sigma_{\mathrm{Landau}}$.

The Bayes Method is based on a statistical combination of the parameterization and the measurement in the calorimeters. This combination is performed using Bayes' theorem. This method uses information from the calorimeters, even when the measurement falls in the peak region. When the calorimeter measurement falls in the tail, the results provided by this method are similar to those obtained by the Hybrid Method. If the measurements falls in the peak region, the measurement still constrains the energy loss pdf, improving the energy loss reconstruction resolution. In addition, this method generalizes the selection procedure of the hybrid method, with an event-by-event optimization and for each calorimeter subsystem. This generalization allows also, in principle, an automatic improvement in the energy loss reconstruction as the calorimeter calibration improves.

The full validation of these methods in muon reconstruction with all muon reconstruction effects is shown in the next section. The most significant of these effects are the intrinsic resolutions of the inner detector and muon spectrometer. However, to validate the methods standalone, it is necessary to do it in a model free of these reconstruction effects.

The Hybrid Method has been validated through the energy loss reconstruction distributions in the ATLAS full simulation using the muon kinematics from the simulation. The ratio of the energy loss resolution for the Hybrid Method, σ_{hybrid}, with respect to the parameterization alone, σ_{param}, is presented in Figure 15. The resolution is defined as the square root of the variance of the energy loss resolution. For low-p_T values the ratio is close to unity, as expected due to the smaller fraction of events in the Landau tail. For increasing p_T values the ratio decreases, approaching 30% at $p_T = 1$ TeV. Thus, using the Hybrid Method results in a significant improvement in the energy loss estimation with respect to the parameterization alone.

In addition, the performance of the Bayesian Method has been studied in a toy model under the assumption that the calorimeter calibration is understood. Muons of 1 TeV were shot through a block of matter representative of one of the samplings of the hadronic calorimeter. A perfect muon spectrometer was assumed as it is done for the Hybrid Method above. Figure 16 shows some results from this study that demonstrate the potential of the Bayesian Method to reconstruct energy loss. The use of the measurement by itself biases the energy loss reconstruction. The Bayesian Method, on the other hand, shows no biases. Incidentally, there are no biases in the energy loss reconstruction if the muon spectrometer measurement is coupled to the energy loss reconstruction in these studies. In addition, the $E_{\mathrm{loss}}^{\mathrm{true}} - E_{\mathrm{loss}}^{\mathrm{reco}}$ distributions show that the resolution obtained with the Bayesian Method is better than that obtained using the parameterization or the measurement only.

These studies prove the potential of these two methods. Now their performance is analyzed when they are used as part of the reconstruction software.

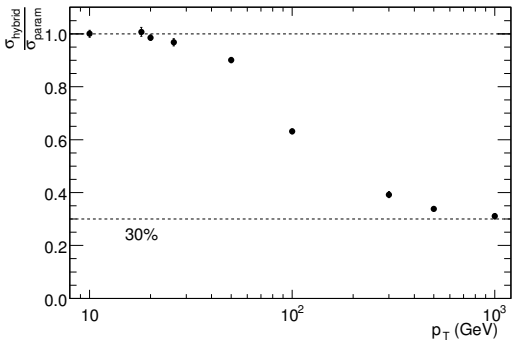

Figure 15: Ratio of the energy loss resolution for the Hybrid Method with respect to the parameterization alone for single muons.

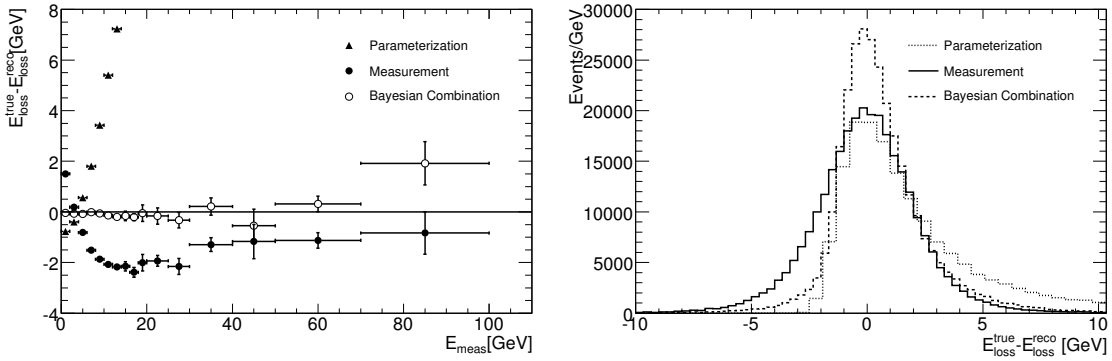

Figure 16: Demonstration of the potential of the statistical method to reconstruct the energy loss. The left plot shows the bias in the energy loss reconstruction, while the right plot shows the $E_{\text{loss}}^{\text{true}} - E_{\text{loss}}^{\text{reco}}$ distribution. Both plots compare the energy loss reconstruction using the parameterization only (triangles, dotted line), the measurement only (filled circles, solid line) and both statistically combined through Bayes' theorem (open circles, dashed line).

3.5 Impact of the Energy Loss Corrections in Reconstruction

Energy loss estimates must be validated as part of the muon reconstruction algorithms. Effects such as the resolution of muon reconstruction, biases intrinsic to the track transport or the effects of gaussian assumptions will be coupled to the energy loss reconstruction. However, the studies shown here are still important for understanding the energy loss correction. They also allow for an investigation of which data samples are most sensitive to an incorrect estimation of the energy loss.

In Figure 17, two parameters that characterize the gaussian distributions $1/p_T^{\text{reco}} - 1/p_T^{\text{true}}$ are shown. In these plots, the label "MS" corresponds to tracks from fits in the muon spectrometer only. The label "MS+E_{loss} correction" refers to tracks reconstructed at the muon spectrometer and transported to the interaction point (IP), applying an energy loss correction (parameterized or hybrid). For Figure 17 the energy loss correction was calculated using the Muonboy parameterization only. The label "MS+ID" refers to tracks reconstructed with the muon spectrometer and the inner detector. To obtain these combined tracks, the energy loss correction needs to be considered in the fit. The distributions are calculated in $1/p_T$-space because the muon spectrometer reconstruction and inner detector reconstruction have gaussian fluctuations in $1/p_T$. These plots refer to muons reconstructed in the barrel ($|\eta| < 1.0$) of the muon spectrometer. In the left plot, the bias in the reconstruction is shown, defined as the mean of the

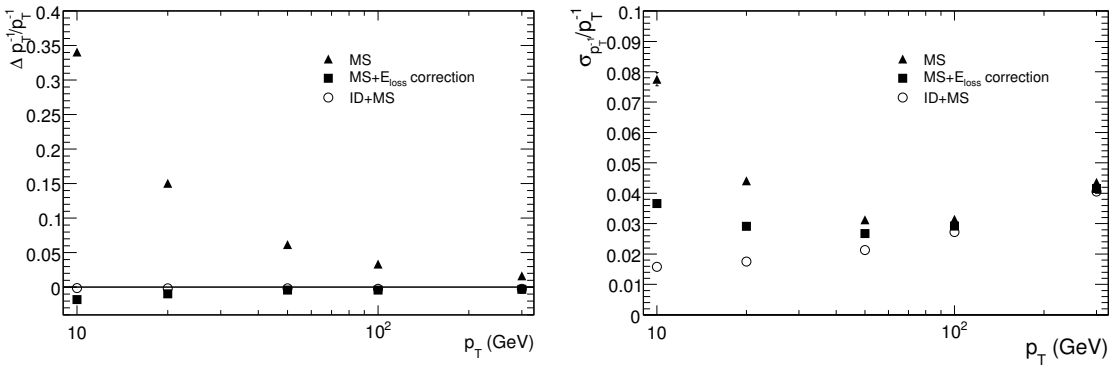

Figure 17: Left: Muon reconstruction bias for different algorithms as a function of muon p_T. Right: Muon reconstruction resolution for different algorithms as a function of muon p_T. These plots were produced with the Muonboy/STACO algorithms for muon reconstruction [1], but similar performance is obtained with the MOORE/Muid algorithms [2, 7].

distribution

$$\frac{\delta p_T^{-1}}{p_T^{-1}} = p_T^{\text{true,IP}} \left(\frac{1}{p_T^{\text{reco}}} - \frac{1}{p_T^{\text{true,IP}}} \right), \tag{4}$$

with $p_T^{\text{true,IP}}$ being the true p_T of the muon at the IP. Clearly, in the absence of an energy loss correction, this reconstruction can be highly biased. Such a bias also causes a degradation in the resolution. The application of an energy loss correction reduces this bias and improves the resolution. Further bias reduction and resolution improvement is obtained by using the inner detector together with the muon spectrometer to reconstruct the muon track. However, the combination of inner detector tracks and muon spectrometer tracks is only possible if a proper energy loss correction exists.

Figure 18 shows the invariant mass resolution ($M_{\text{inv}}^{\text{reco}} - M_{\text{inv}}^{\text{true}}$) for $Z \to \mu\mu$ and $Z'(1000\ \text{GeV}) \to \mu\mu$ samples. The events include a generation cut that requires the p_T of both decay muons to be above 7 GeV

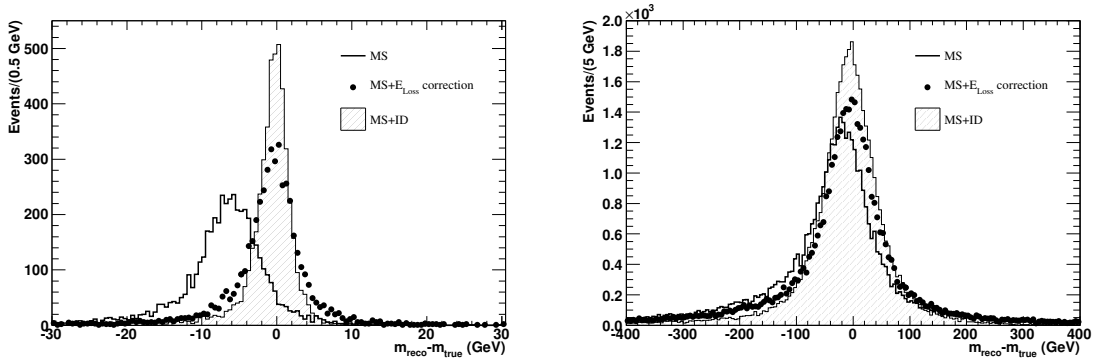

Figure 18: Left: Reconstruction resolution of the Z peak for different algorithms. Right: Reconstruction resolution of the Z' peak for a $Z' \to \mu\mu$ of mass 1 TeV for different algorithms. These plots were produced with the MOORE/Muid algorithms for muon reconstruction [2, 7], but similar performance is obtained with the Muonboy/STACO algorithms [1].

for Z decays and above 20 GeV for Z' decays. Inner detector and muon spectrometer tracks were required for both reconstructed muons. The effect of the energy loss correction is most significant in the Z-mass reconstruction. If the energy loss is not included a shift of about 7 GeV in the mass peak and a significant

deterioration in the resolution are visible. These effects are much less pronounced in the reconstruction of the Z' peak. This happens because the more energetic muons from the Z' lose a smaller fraction of their total energy as they pass through the calorimeters.

An additional improvement in the Z and Z' resolution is possible if the energy loss correction uses the calorimeter measurement [20]. This is demonstrated in Figure 19, where a comparison is shown

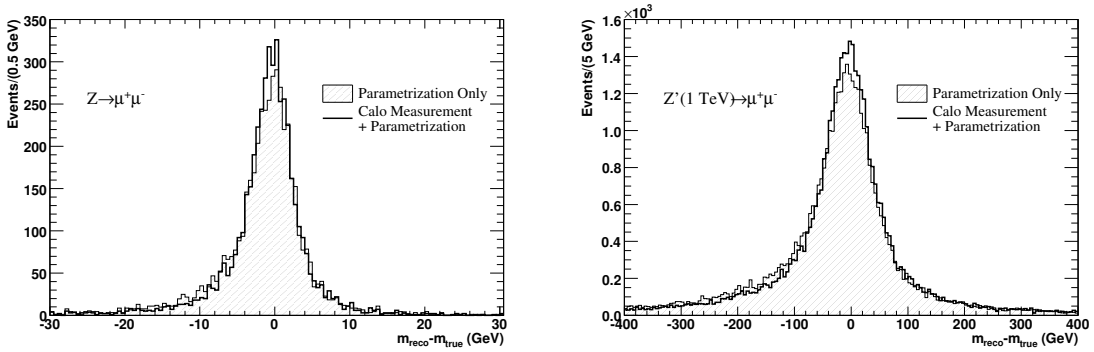

Figure 19: Left: Reconstruction resolution of the Z peak for an algorithm using muon spectrometer standalone tracks and the parameterized energy loss correction (filled histogram) and an algorithm using a combination of a parameterization and the calorimeter measurement for the energy loss correction (empty histogram). Right: Reconstruction resolution of the Z' peak for a $Z' \to \mu\mu$ of mass 1 TeV for the same algorithms.

for the muon spectrometer reconstruction with energy loss correction with and without the calorimeter measurement. The same samples as for Figure 18 were used. A few events are recovered from the tails and populate the peak region. This results in $\approx 8\%$ resolution improvement when the inner detector hits are not used. If the inner detector hits are used the resolution improves by $\approx 4\%$, showing that the combined fit is less sensitive to the energy loss correction. These plots were produced with the MOORE/Muid algorithms for muon reconstruction using the Hybrid Method (see Section 3.4). A similar performance is expected using the Bayesian Method, implemented in the ATLAS tracking.

4 Tagging of Muons in the Calorimeters

In this section the different calorimeter-based muon identification algorithms are described. Section 4.1 provides a detailed description of the algorithm that is currently part of the standard reconstruction; and Section 4.2 illustrates its performance in different physics samples.

These algorithms have been developed with the main goal of complementing the muon spectrometer in two ways: recovering muons with low transverse momentum (p_T = 2-5 GeV), and in the regions of limited spectrometer acceptance (especially in the $\eta \sim 0$ region). For completeness, algorithms used for commissioning or triggering are also discussed.

There are two types of calorimeter-based muon tagging algorithms. Their main difference lies in how they initiate the muon search. The calorimeter-seed algorithms search for muons looking at the measured energy. Cells with energy depositions inside some energy range are used as seeds. The lower limit of this range is known as the *initiation* threshold. The cluster of cells used to identify the muon is then built up by adding cells around the seed cell whose energy is above a second lower threshold, so called *continuation* threshold. At the end of the clustering, the η and ϕ directions of the reconstructed cluster can be used to match a track in the inner detector. There are two algorithms that correspond to this description:

- `LArMuID` is based on a topological clustering algorithm used by ALEPH [21]. A topological clustering algorithm groups neighboring cells whose energy is above a given threshold. Therefore, the resulting clusters have a variable number of cells. This algorithm was used to find muons using the electromagnetic calorimeter data during the test beam and the cosmic commissioning data analysis. It builds the cluster from a seed cell in the middle sampling of the electromagnetic calorimeter. Then, it creates the cluster adding another cell (if any) adjacent in ϕ above the continuation threshold. Due to the accordion structure of the electromagnetic calorimeters there are no more than two adjacent cells in ϕ that can share the muon signal, thus the clusters consist of at most two cells. The efficiency was measured with a muon beam during the combined test beam as the fraction of events with a reconstructed muon cluster. The efficiency and the probability to generate a fake muon from noise fluctuations were evaluated as a function of both thresholds. The clustering algorithm inherently biases the energy reconstruction, so the lower the thresholds the better the estimation of the reconstructed energy for the muon. The spectrum of energies collected has been compared to and shown agreement with GEANT4.

- `TileMuId` is simple and fast and is used for triggering purposes. Its clustering methods are similar to those of `LArMuID`. This algorithm, however, runs by default as part of the reconstruction software. It starts with a search for a "candidate" muon in the cells belonging to the last TileCal sampling, where the muon gives the clearest signature, due to the screening effect of the two previous samplings. If the measured energy is between a lower and and upper threshold, it uses the η and ϕ coordinates of the cell to look for another cell with energy within the same thresholds in the central sampling. If both searches are successful it looks for a third cell with energy within the thresholds in the first sampling. When cells with energies within the thresholds are found in all three samplings, the candidate is confirmed to be a muon. Performance studies of `TileMuId` can be found in [22].

There are two track-seed algorithms that extrapolate inner detector tracks through the calorimeter identifying those matching the energy deposition pattern of a muon. The track-seed algorithms use no tracking information from the muon spectrometer. The first track-seed algorithm, `CaloMuonTag`, will be described in detail in the next section.

The second track-seed algorithm, `CaloMuonLikelihoodTool`, builds a likelihood ratio to discriminate muons from pions. The likelihood discriminant is built out of different energy ratios in order to capture the global features of the energy depositions. The discrimination power of these ratios varies both as a function of the momentum of the particles considered, and as a function of η. Therefore three bins in η (barrel, crack, end-cap) and three bins in momentum (0-10 GeV, 10-50 GeV, 50-100 GeV) are used, and a different set of ratios is selected for each of the 9 regions. The likelihood ratio for the muon candidate is then defined as

$$\mathscr{L}(x_1,...,x_N) = \prod_{i=1}^{N} \frac{P_i^{\mu}(x_i)}{P_i^{\mu}(x_i) + P_i^{\pi}(x_i)}. \tag{5}$$

Where P_i^{μ} and P_i^{π}, $i = 1,...,N$ are the pdf for the energy ratios. The performance of this algorithm is still being studied, however, the first results show that it is comparable to the performance of `CaloMuonTag` discussed in Section 4.2.

4.1 CaloMuonTag

`CaloMuonTag` extrapolates inner detector tracks through the calorimeters, collecting the energy in the cell closest to the extrapolated track for each traversed sampling. The muon can deposit energy in more than one cell in the hadronic calorimeter, but the probability of this happening is rather low, as illustrated in Figure 20. For the purpose of this algorithm, it is enough to assume that all the energy deposited by

the muon is localized in the central cell. This also minimizes the electronic noise, which is particularly large in the HEC.

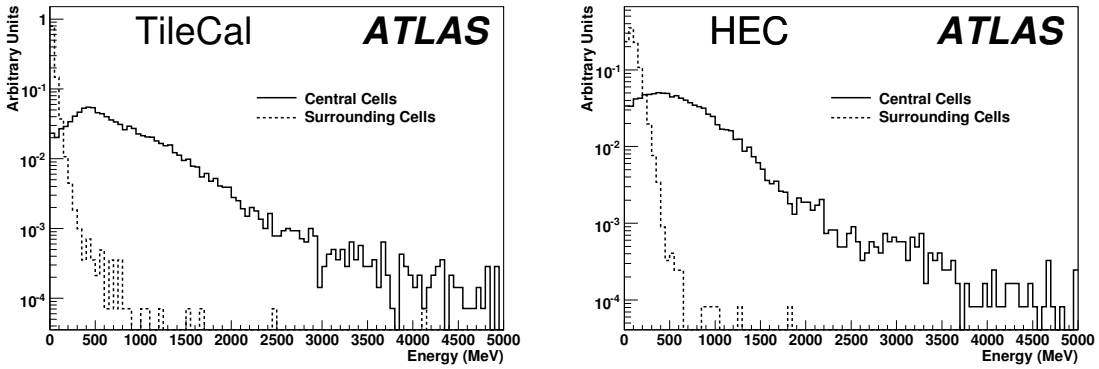

Figure 20: Energy found in the cell traversed by the extrapolated track (solid line) and the surrounding cells (dashed line) in the TileCal (left) and in the HEC (right). Distributions obtained for momentum 100 GeV muons.

A track preselection is made to reduce the number of fakes in the output of the algorithms. In addition, this preselection reduces the time needed by the algorithm to run on events with high track multiplicity. The following cuts in p_T, and transverse isolation energy (E_T^{iso}) inside a cone of 0.45 are applied:

- $p_T > 2$ GeV and $E_T^{\text{iso}} < 10$ GeV for tracks pointing to the barrel ($\eta < 1.6$).
- $p_T > 3$ GeV and $E_T^{\text{iso}} < 8$ GeV for tracks pointing to the end-cap.

Tracks are rejected if any of the collected energies are above veto values defined for each sampling. As most fakes are seeded by low-p_T tracks, more stringent cuts can be set for low-p_T (< 10 GeV) track candidates. These cuts can be relaxed for track candidates of higher p_T.

Once calorimeter cells along the muon trajectory have been identified, the algorithm determines the lower threshold energy cut that should be used for the tagging as a function of η:

- $E_{\text{th}} = \frac{E_0^{\text{barrel}}}{\sin^2\theta}$ for $|\eta| < 1.7$,
- $E_{\text{th}} = \frac{E_0^{\text{end-cap}}}{(1-\sin\theta)^2}$ for $|\eta| > 1.7$,

where θ is the polar angle. The values of E_{th} from these two equations roughly follow the shape of the measured energy distributions, which increases with the path length of the muon in the cell.

Energy depositions in the last sampling of the calorimeters give the most reliable muon signals. However, due to the gap between the TileCal barrel and extended barrel modules, and the transition region between the TileCal and the end-cap (HEC) calorimeters, it is necessary to look in the two previous samplings to obtain a good efficiency throughout η. For this reason, if the energy in the last sampling, or one of the two previous samplings depending on the η of the track, is above the threshold cut, E_{th}, the track is tagged as a muon. A different tag is given depending on which sampling passes the threshold cut.

4.2 Performance

In this section the performance of `CaloMuonTag` is analyzed. The performance of `CaloMuonTag` is studied in some relevant physics samples:

- $pp \rightarrow J/\psi \rightarrow \mu\mu$. A direct production of a J/ψ decaying to two muons with the following cuts at generation level: one muon with $p_T > 6$ GeV and the other with $p_T > 4$ GeV.
- $H \rightarrow ZZ^* \rightarrow 4\ell$. A Higgs generated with an invariant mass of 130 GeV is forced to decay into two Z's (one of them offshell) that decay leptonically. Only events with four muons are used for reconstructing the Higgs peak, but all events are used for the efficiency/fake rate calculation.
- $t\bar{t}$. A sample of pair produced top quarks with all decay channels allowed.
- $Zbb \rightarrow 4\ell$. A Z is produced in association with 2 b quarks, and is forced to decay into two charged leptons. The b quarks are also forced to decay into electrons or muons.

All samples were generated with pile-up with a safety factor of 5, i.e. five times nominal value expected at a luminosity of $10^{33} cm^{-2} s^{-1}$. Except for the $pp \rightarrow J/\psi \rightarrow \mu\mu$ sample, where a safety factor of 2 was used.

Figure 21 shows the performance of the calorimeter muon tagger algorithm on selected samples. The

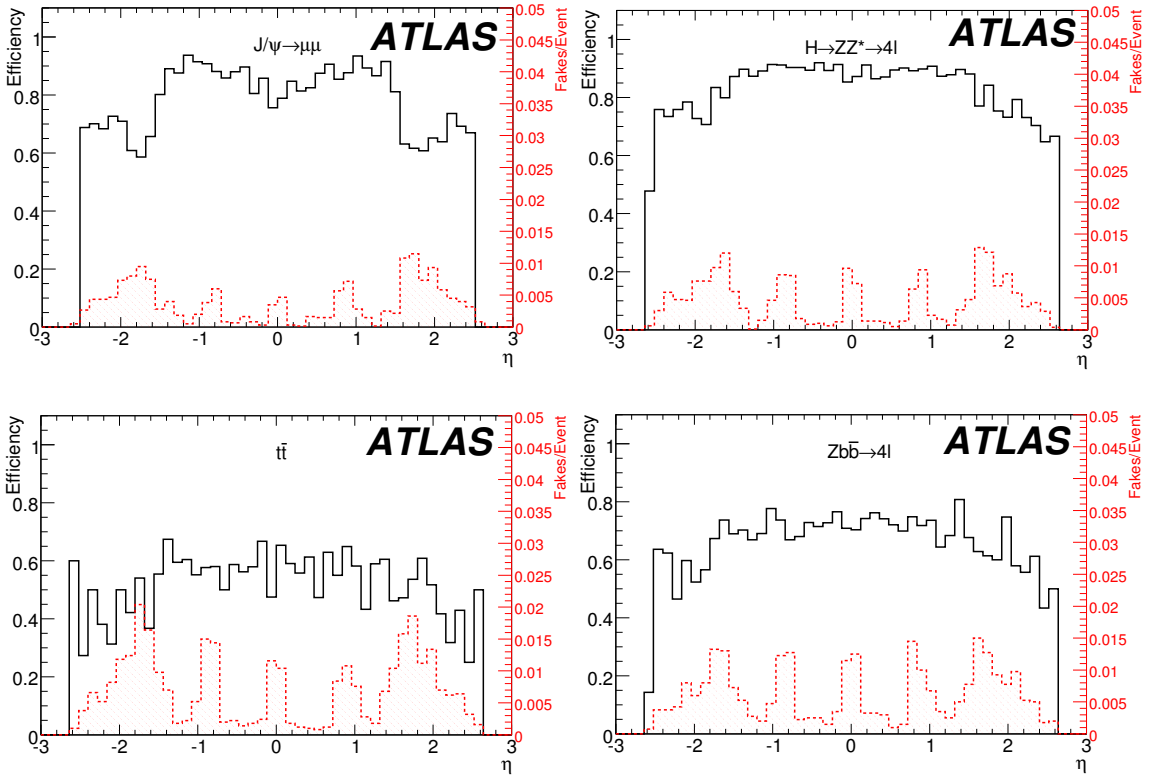

Figure 21: Efficiency (and fakes per event, right axis in red and shaded histograms) vs η for different samples. Top left: $pp \rightarrow J/\psi \rightarrow \mu\mu$. Top right: $H(130) \rightarrow ZZ^* \rightarrow 4\ell$. Bottom left: $t\bar{t}$. Bottom right: $Zbb \rightarrow 4\ell$.

vertical axis on the left shows the efficiency (top distributions). The vertical axis on the right (in red) shows the fake rate (the number of misidentified tracks per event), represented by the shaded distribution at the bottom of the plots. The efficiency (fake rate) is defined as the fraction of muons that are found by the algorithm and (not) matched with a true MC muon. Muons from minimum-bias interactions were not included in the efficiency calculation.

For the $t\bar{t}$ ($Zbb \to 4\ell$) sample, the algorithm performs well in identifying isolated muons from W's (Z's). However, due to the isolation and veto cuts applied to reduce the number of fakes, the efficiency for non-isolated muons from b quarks is very poor, affecting the overall efficiency.

To reduce the fake rate due to the low-p_T tracks in the end-caps, some efficiency in that region needs to be sacrificed. The "peaks" in the fake rate in η match the regions where the acceptance of the last calorimeter sampling is limited, and the two previous samplings are used for muon identification. Due to the higher electronic noise, `CaloMuonTag` presents a higher fake rate in the HEC than in the TileCal. The results for these samples, and for dijet samples generated with different p_T transfers at the hard scattering interaction are summarized in Table 1.

	$J/\psi \to \mu\mu$	$H \to 4\ell$	$t\bar{t}$	$Zbb \to 4\ell$	1120-2240	560-1120	280-560	70-140	17-35
Eff.	0.80	0.86	0.54	0.69	-	-	-	-	-
f/e	0.05	0.09	0.16	0.14	0.11	0.12	0.12	0.13	0.12

Table 1: Summary of the efficiencies and fakes per event (f/e) for different physics processes and dijet samples (top numbers show the ranges of p_T transfers at the hard scattering interaction, in GeV).

Finally, Figures 22 and 23 are used to evaluate the performance improvement when using calorimeter muons to reconstruct the Higgs and the J/ψ mass. The plots on the left show the invariant mass reconstructed with muons from a combined muon reconstruction algorithm, which makes use of both inner detector and muon spectrometer tracks. The plots on the right show the invariant mass including muons tagged by `CaloMuonTag` with momenta reconstructed by the inner detector.

To obtain the plots in Figure 22 the same set of cuts were used as in the $H(130) \to ZZ^* \to 4\ell$ stud-

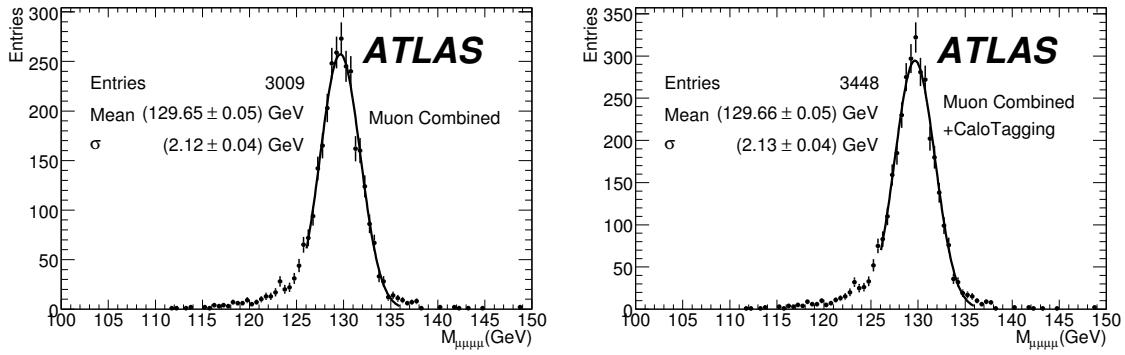

Figure 22: Reconstructed Higgs peak in the $H \to 4\ell$ invariant mass reconstruction for the standard combined muons (left) and for combined muons together with inner detector muons tagged by `CaloMuonTag` in the η region $|\eta| < 0.1$ (right).

ies [19]. The increase on the number of reconstructed events was achieved by adding an extra muon found by the `CaloMuonTag` algorithm during the muon preselection. The extra muon was requested to be found in the last sampling of the TileCal and within the $|\eta| < 0.1$ region. No loss in mass resolution or shift in the mean of the mass peak are observed between the two selected muon samples. The acceptance gap around $|\eta| < 0.1$ represents 4% of the $|\eta| < 2.5$ region covered by the combined muon reconstruction. Since, four muons are recontructed in this analysis, the total efficiency loss due to the gap is 16%. This results shows that calorimeter identification can recover almost all of the lost events (14.9%).

For the plots shown in Figure 23 the muons used to reconstruct the invariant mass peak were matched

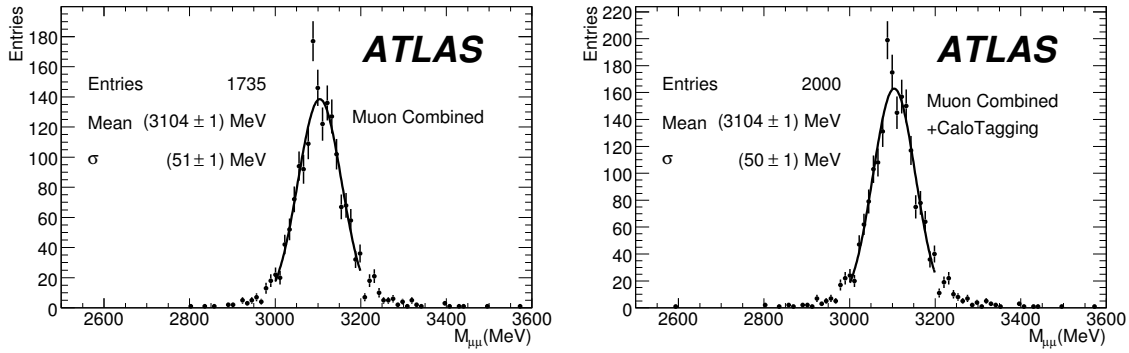

Figure 23: Reconstructed J/ψ peak in the $J/\psi \to \mu\mu$ invariant mass reconstruction for standard combined muons (left) and for combined muons together with inner detector muons tagged by `CaloMuonTag` in the η region $|\eta| < 0.1$ (right).

to the Monte Carlo truth. In this case, all muons identified by the calorimeter were added to the combined reconstruction muons. Again, no loss in mass resolution or shift in the mean of the mass peak are observed between the two selected muon samples.

`CaloMuonTag` shows very good efficiency and acceptable fake rate for a high-p_T analysis like $H \to ZZ^* \to 4\mu$. An additional 15% of events were reconstructed when muons identified by `CaloMuonTag` were added to the muons found by the standard reconstruction algorithm. In low-p_T analyses, such as $J/\psi \to 2\mu$, tighter selection cuts need to be applied to keep an acceptable fake rate. This reduces the efficiency of the tagging algorithms. However, an additional 15% of events were reconstructed when muons from `CaloMuonTag` were also used.

5 Conclusion

This document reviews the current status of the understanding of muon energy loss in the ATLAS calorimeters. Although energy losses and their distribution along the muon track have a very small impact on muon reconstruction inside the muon system, they play an important role in the transport of a reconstructed muon track to the beam pipe. During this backtracking, the muon momentum can be corrected using the energy measured in the calorimeter cells traversed. This procedure is justified for muons that have a catastrophic energy loss. In most cases, the muon momentum can be corrected using a parameterization of energy loss, estimated from the reconstructed momentum and the amount and the nature of the material traversed by the reconstructed trajectory. Techniques that attempt to combine the measurement with the parameterization to improve the energy loss estimate have been developed and validated. A performance improvement is achieved in some important analyses through the use of these techniques.

Muon tagging algorithms that use calorimeter measurements and track information have been presented. These algorithms have been developed with the main goal of complementing the muon spectrometer in two ways: recovering muons with very low transverse momentum, and in the regions of limited spectrometer acceptance, especially in the $\eta \sim 0$ region. The performance of the calorimeter muon tagger algorithm in a few relevant data samples has been shown.

6 Acknowledgments

We acknowledge the support of the European Commission, through the ARTEMIS Research Training Network.

References

[1] S. Hassani et al., Nucl. Instr. and Meth. A **572** (2007) 77.

[2] T. Lagouri et al., IEEE Trans. Nucl. Sci. **51** (2004) 3030.

[3] K. Nikolopoulos et al., Muon Energy Loss Upstream of the Muon Spectrometer, ATLAS Note ATL-MUON-PUB-2007-002.

[4] V.L. Highland, Nucl. Instr. and Meth. **129** (1975) and Nucl. Instr. and Meth. **161** (1979).

[5] R. Frühwirth et al., Nucl. Instr. and Meth. A **262** (1987).

[6] T. Cornelissen et al., Concepts, Design and Implementation of the ATLAS New Tracking (NEWT), ATLAS Note ATL-SOFT-PUB-2007-007.

[7] D. Adams et al., Track Reconstruction in the ATLAS Muon Spectrometer with Moore, ATLAS Note ATL-SOFT-2003-007 (2003).

[8] The GEANT4 Collaboration, S.Agostinelli et al., Nucl. Instr. and Meth. A **506** (2003) 250.

[9] W. Lohmann, R. Kopp and R. Voss, Energy Loss of Muons in the Energy Range 1-10000 GeV, CERN 85-03 (1985).

[10] W.-M. Yao et al., Journal of Physics G **33** (2006) 1.

[11] D. López Mateos, E. W. Hughes and A. Salzburger, A Parameterization of the Energy Loss of Muons in the ATLAS Tracking Geometry, ATLAS Note ATL-MUON-PUB-2008-002.

[12] A. Salzburger, S. Todorova and M. Wolter, The ATLAS Track Extrapolation Package, ATLAS Note ATL-SOFT-PUB-2007-004.

[13] H. Bischel, Rev. Mod. Phys. **60** (1988) 663.

[14] C. Cojocaru et al., Muon Results from the EMEC/HEC Combined Run corresponding to the ATLAS Pseudorapidity Region $1.6 < |\eta| < 1.8$, ATLAS Note ATL-LARG-PUB-2004-006.

[15] ATLAS Collaboration, ATLAS Liquid Argon Calorimeters Technical Design Report, CERN/LHCC/96-41 (1996).

[16] T. Davidek and R. Leitner, Parametrization of the Muon Response in the Tile Calorimeter, ATLAS Note ATL-TILECAL-97-114.

[17] ATLAS Collaboration, ATLAS Tile Calorimeter Technical Design Report, CERN/LHCC/96-42 (1996).

[18] G. Schlager, The Energy Response of the ATLAS Calorimeter System, CERN-THESIS-2006-056.

[19] The ATLAS Collaboration, Search for the Standard Model $H \rightarrow ZZ^* \rightarrow 4l$, this volume.

[20] K. Nikolopoulos et al., IEEE Trans. Nucl. Sci. **54** (2007) 1792.

[21] J. P. Albanese, E. Kajfasz and P. Payre, Nucl. Instr. and Meth. A **253** (1986) 73.

[22] The ATLAS Collaboration, Performance of the Muon Trigger Slice with Simulated Data, this volume.